The Astrophysical Journal Letters, 971:L25 (8pp), 2024 August 10 https://doi.org/10.3847/2041-8213/ad6607


# Discovery of a Hypervelocity L Subdwarf at the Star/Brown Dwarf Mass Limit

Adam J. Burgasser[1], Roman Gerasimov[2], Kyle Kremer[3], Hunter Brooks[4], Efrain Alvarado, III[5], Adam C. Schneider[6], Aaron M. Meisner[7], Christopher A. Theissen[1], Emma Softich[1], Preethi Karpoor[1], Thomas P. Bickle[8,9], Martin Kabatnik[9], Austin Rothermich[10,11,12], Dan Caselden[10], J. Davy Kirkpatrick[13], Jacqueline K. Faherty[10], Sarah L. Casewell[14], and Marc J. Kuchner[15]
The Backyard Worlds: Planet 9 Collaboration

[1] Department of Astronomy & Astrophysics, UC San Diego, La Jolla, CA, USA; aburgasser@ucsd.edu
[2] Department of Physics & Astronomy, University of Notre Dame, Notre Dame, IN 46556, USA
[3] TAPIR, California Institute of Technology, Pasadena, CA 91125, USA
[4] Department of Astronomy and Planetary Science, Northern Arizona University, Flagstaff, AZ 86011, USA
[5] Department of Astronomy, University of California, Berkeley, CA 94720-3411, USA
[6] US Naval Observatory, Flagstaff Station, Flagstaff, AZ, USA
[7] NSF National Optical-Infrared Astronomy Research Laboratory, 950 North Cherry Avenue, Tucson, AZ 85719, USA
[8] School of Physical Sciences, The Open University, Milton Keynes, MK7 6AA, UK
[9] Backyard Worlds: Planet 9, USA
[10] Department of Astrophysics, American Museum of Natural History, Central Park West at 79th Street, NY 10024, USA
[11] Department of Physics, Graduate Center, City University of New York, 365 5th Ave., New York, NY 10016, USA
[12] Department of Physics and Astronomy, Hunter College, City University of New York, 695 Park Avenue, New York, NY, 10065, USA
[13] IPAC, Mail Code 100-22, Caltech, 1200 East California Boulevard, Pasadena, CA 91125, USA
[14] Centre for Exoplanet Research, School of Physics and Astronomy University of Leicester, University Road, Leicester, LE1 7RH, UK
[15] Exoplanets and Stellar Astrophysics Laboratory, NASA Goddard Space Flight Center, 8800 Greenbelt Road, Greenbelt, MD 20771, USA
*Received 2024 May 27; revised 2024 July 4; accepted 2024 July 8; published 2024 August 8*

## Abstract

We report the discovery of a high-velocity, very low-mass star or brown dwarf whose kinematics suggest it is unbound to the Milky Way. CWISE J124909.08+362116.0 was identified by citizen scientists in the Backyard Worlds: Planet 9 program as a high-proper-motion ($\mu = 0\farcs9\ \mathrm{yr}^{-1}$) faint red source. Moderate-resolution spectroscopy with Keck/NIRES reveals it to be a metal-poor early L subdwarf with a large radial velocity ($-103 \pm 10\ \mathrm{km\ s}^{-1}$), and its estimated distance of $125 \pm 8$ pc yields a speed of $456 \pm 27\ \mathrm{km\ s}^{-1}$ in the Galactic rest frame, near the local escape velocity for the Milky Way. We explore several potential scenarios for the origin of this source, including ejection from the Galactic center $\gtrsim$3 Gyr in the past, survival as the mass donor companion to an exploded white dwarf, acceleration through a three-body interaction with a black hole binary in a globular cluster, and accretion from a Milky Way satellite system. CWISE J1249+3621 is the first hypervelocity very low-mass star or brown dwarf to be found and the nearest of all such systems. It may represent a broader population of very high-velocity, low-mass objects that have undergone extreme accelerations.

*Unified Astronomy Thesaurus concepts:* Globular star clusters (656); Hypervelocity stars (776); L subdwarfs (896); Metallicity (1031); Type Ia supernovae (1728); Low mass stars (2050); Galactic archaeology (2178)

## 1. Introduction

The majority of stars in the neighborhood of the Sun have low relative velocities ($v \approx 10$–$30\ \mathrm{km\ s}^{-1}$), reflecting their common origin in star-forming clusters concentrated in the plane of the Milky Way. A rare subset of nearby stars has much higher velocities ($v_{\tan} \gtrsim 400\ \mathrm{km\ s}^{-1}$; <0.3% of stars within 1 kpc; Favia et al. 2015). These stars may originate from the Milky Way's ancient halo population or underwent strong dynamical interactions with compact objects such as the Milky Way's central supermassive black hole (Hills 1988) of compact binaries in dense clusters (Yu & Tremaine 2003; Fragione & Gualandris 2019), or they may be the survivors of the supernova explosion of a binary companion (Blaauw 1961; Portegies Zwart 2000). The fastest "hypervelocity" stars are unbound to the Milky Way's gravitational potential and may even have extragalactic origins (Abadi et al. 2009; Piffl et al. 2011). These rare objects trace extreme interactions that may be explored through their trajectories, velocity distributions, and atmospheric properties (Brown 2015).

The Gaia mission (Gaia Collaboration et al. 2021) has greatly expanded our sample of high-velocity stars by providing 5D (position, parallax, and proper motion) or 6D (plus radial velocity (RV)) coordinates for billions of stars out to kiloparsec distances. These measurements, combined with detailed chemical abundances from RAVE (Steinmetz et al. 2006), LAMOST (Cui et al. 2012), APOGEE (Majewski et al. 2017), and other spectral surveys, have enabled the discovery and characterization of over a dozen hypervelocity stars (e.g., Du et al. 2019; Quispe-Huaynasi et al. 2022; Liao et al. 2023; Scholz 2024) that originate from environments as diverse as the Galactic center, globular clusters (GCs), or satellite systems. Current studies focus on deep optical measurements of rare and distant stars and primarily sample main-sequence and red giant stars over a limited range of mass ($0.7\,M_\odot \lesssim M \lesssim 2\,M_\odot$) and age ($\lesssim$1 Gyr for high-velocity OB stars), which may limit our ability to probe compositions and origins.

The citizen science project Backyard Worlds: Planet 9 (BYW; Kuchner et al. 2017) takes advantage of multiepoch

**Table 1**
Properties of J1249+3621

| Property | Value | References |
|---|---|---|
| $\alpha_{J2000}$ | $12^h49^m09\overset{s}{.}08$ | (1) |
| $\delta_{J2000}$ | $+36°21'16''$ | (1) |
| $\mu_\alpha \cos\delta$ | $344 \pm 5$ mas yr$^{-1}$ | (2, 3) |
| $\mu_\delta$ | $-814 \pm 5$ mas yr$^{-1}$ | (2, 3) |
| $i$ (AB) | $21.48 \pm 0.15$ mag | (2) |
| $z$ (AB) | $20.01 \pm 0.06$ mag | (2) |
| $y$ (AB) | $19.13 \pm 0.05$ mag | (2) |
| $J$ (Vega) | $17.10 \pm 0.03$ mag | (3) |
| $K$ (Vega) | $16.46 \pm 0.04$ mag | (3) |
| $W1$ (Vega) | $15.92 \pm 0.04$ mag | (1) |
| $W2$ (Vega) | $15.59 \pm 0.07$ mag | (1) |
| SpT | sdL1 | (4) |
| $d_{est}$[a] | $125 \pm 8$ pc | (4) |
| $v_{tan}$ | $524 \pm 33$ km s$^{-1}$ | (4) |
| $T_{eff}$[b] | 1715–2320 K | (4, 5, 6) |
| log $g$[b] | 4.4–5.1 (cm s$^{-2}$) | (4, 5, 6) |
| [M/H][b] | $-1.4$ to $-0.5$ | (4, 5, 6) |
| [$\alpha$/Fe] | $+0.25 \pm 0.07$ | (4, 5) |
| Est. Mass | $0.082^{+0.002}_{-0.003}$ $M_\odot$ | (4, 7) |
| $RV$ | $-103 \pm 10$ km s$^{-1}$ | (4) |
| $U_{LSR}$[c] | $449 \pm 28$ km s$^{-1}$ | (4) |
| $V_{LSR}$[c] | $-292 \pm 19$ km s$^{-1}$ | (4) |
| $W_{LSR}$[c] | $-15 \pm 11$ km s$^{-1}$ | (4) |
| $v_{GRF}$[d] | $456 \pm 27$ km s$^{-1}$ | (4) |

**Notes.**
[a] Estimated from the spectral classification, *JKW1W2* photometry, and the spectral-type/absolute magnitude relations of Gonzales et al. (2018) and Zhang et al. (2019).
[b] Based on the $\pm1\sigma$ range of Elf Owl and SAND model fits.
[c] LSR velocities assuming a solar motion from Schönrich et al. (2010).
[d] GRF speed assuming $v_{circ} = 220$ km s$^{-1}$ at the Solar radius.
**References:** (1) CatWISE2020 (Marocco et al. 2021) at astrometric epoch 2015 May 28 (UT); (2) PanSTARRS (Chambers et al. 2016); (3) UKIRT Hemisphere Survey (Dye et al. 2018); (4) This Letter; (5) Alvarado et al. (2024); (6) Mukherjee et al. (2024); (7) Gerasimov et al. (2024).

infrared photometry and astrometry from the Wide-field Infrared Survey Explorer (WISE; Wright et al. 2010) and its extended NEOWISE mission (Mainzer et al. 2014) to search for faint, infrared moving sources identified by a community of citizen scientists. BYW is ideally designed to find low-mass, high-velocity stars and brown dwarfs, including local low-temperature metal-poor subdwarfs—the L, T, and Y subdwarfs—from the thick disk and halo populations (Meisner et al. 2020, 2021; Schneider et al. 2020; Kirkpatrick et al. 2021a; Brooks et al. 2022; Burgasser et al. 2024). In this Letter, we report the discovery of a nearby, metal-poor L subdwarf, CWISE J124909.08+362116.0 (hereafter J1249+3621), whose speed may exceed the local escape velocity of the Milky Way, making it the first low-mass hypervelocity star and the nearest such system to the Sun.

## 2. Identification and Spectral Observations

J1249+3621 was identified by citizen scientists Tom Bickle, Martin Kabatnik, and Austin Rothermich in multiepoch unWISE images (Lang 2014; Meisner et al. 2018; Schlafly et al. 2019) on the BYW citizen science portal.[16] Its $W2$ magnitude and $J-W2$ color (Table 1) suggest an early-type L dwarf at an estimated distance of ≈100 pc (Kirkpatrick et al. 2021b). Combining astrometry from PanSTARRS (Chambers et al. 2016) and the UKIRT Infrared Deep Sky Survey Hemisphere Survey (UHS; Dye et al. 2018) yields a proper motion of $\mu = 884 \pm 5$ mas yr$^{-1}$, suggesting a tangential velocity of $v_{tan} \approx 420$ km s$^{-1}$ and making it a high-priority target for spectroscopic follow-up.

J1249+3621 was observed on 30 January 2024 (UT) in clear and windy conditions with the Near-Infrared Echellette Spectrometer (NIRES; Wilson et al. 2004) on the Keck II 10 m telescope, a cross-dispersed spectrograph that provides $\lambda/\Delta\lambda \approx 2700$ spectra over 0.9–2.45 $\mu$m. We obtained six exposures of 300 s each at an average airmass of 1.06 with the slit aligned with the parallactic angle. Exposures were made in an ABBA pattern, nodding 10″ along the slit for background subtraction. We also observed the A0 V star HD 108140 ($V = 9.35$) at a similar airmass and dome flat lamp exposures at the start of the night for pixel response calibration. Data were reduced using a modified version of the Spextool package (Cushing et al. 2004), following the procedure of Vacca et al. (2003) for flux calibration and telluric absorption correction.

## 3. Analysis

### 3.1. Classification and Atmosphere Parameters

Figure 1 compares a smoothed version of our spectrum to near-infrared spectral standards from the SpeX Prism Library Analysis Toolkit (SPLAT; Burgasser & Splat Development Team 2017). J1249+3621 exhibits the characteristic features of L-type dwarfs, with strong $H_2O$ absorption at 1.4 and 1.9 $\mu$m and FeH, Na I, and K I absorption in the 1.0–1.3 $\mu$m region. Its NIR spectral slope is distinctly bluer than normal L dwarf spectra, and its 2.3 $\mu$m CO band is highly suppressed, indicating enhanced $H_2$ collision-induced absorption in a low-metallicity, low-temperature atmosphere (Linsky 1969; Burgasser et al. 2003). Indeed, the spectrum of J1249+3621 best matches that of the L subdwarf 2MASS J17561080+2815238 (sdL1; Kirkpatrick et al. 2010) but is somewhat bluer, while it is not as blue as the extreme L subdwarf WISE J043535.80+211509.2 (esdL1; Luhman & Sheppard 2014; Zhang et al. 2017). We classify J1249+3621 as sdL1 based on comparison to a broad range of dwarf and subdwarf spectra. This classification, WISE $W1W2$ and UHS $JK$ Vega magnitudes, and the spectral-type/absolute magnitude relations for L subdwarfs from Gonzales et al. (2018) and Zhang et al. (2019) allow us to estimate a spectrophotometric distance[17] of $125 \pm 8$ pc for J1249+3621, implying $v_{tan} = 524 \pm 33$ km s$^{-1}$.

To further evaluate its physical properties, we compared the smoothed spectrum of J1249+3621 to the Sonora Elf Owl (Mukherjee et al. 2024) and Spectral ANalog of Dwarfs (SAND; Alvarado et al. 2024) atmosphere models. These models encompass the temperatures ($1500\,\mathrm{K} \lesssim T_{eff} \lesssim 2400$ K) and subsolar metallicities ([M/H] $\lesssim -0.5$) of L subdwarfs and contain up-to-date opacities and treatments for condensation and disequilibrium chemistry. We used a Metropolis–Hastings Markov Chain Monte Carlo (MCMC) fitting algorithm (Metropolis et al. 1953; Hastings 1970) to fit the models to

[16] http://www.backyardworlds.org

[17] This estimate takes into account photometric uncertainties, uncertainties in the absolute magnitude/spectral-type relations, and a ±1 subtype uncertainty on the classification. We used the uncertainty-weighted mean across all bands and both relations, which are in formal agreement within the uncertainties.

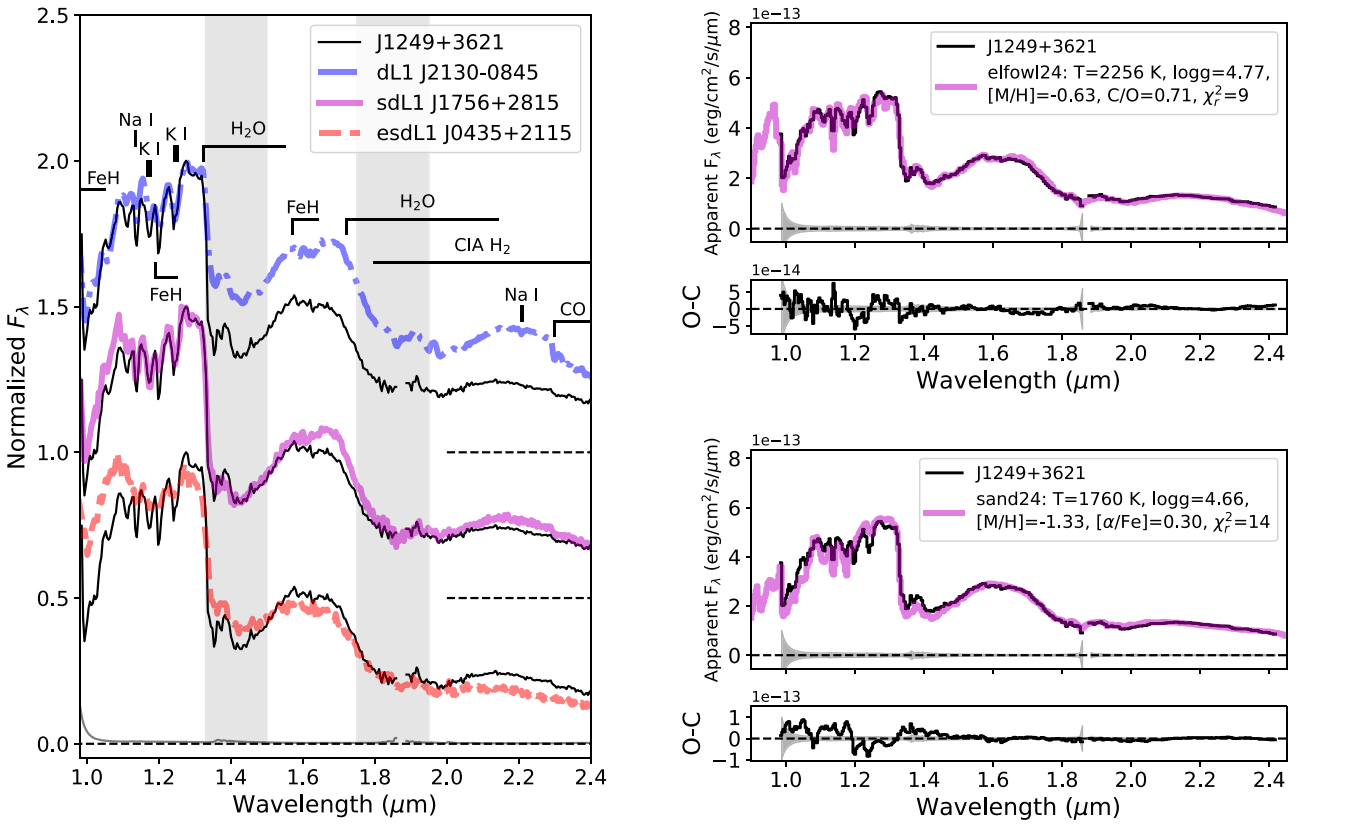


**Figure 1.** Left: Keck/NIRES spectrum of J1249+3621 smoothed to a resolution of $\lambda/\Delta\lambda = 150$ (black lines), compared to the L dwarf templates 2MASSW J2130446-084520 (L1, blue dotted–dashed line; data from Bardalez Gagliuffi et al. 2014), 2MASS J17561080+2815238 (sdL1, magenta line; data from Kirkpatrick et al. 2010), and WISE J043535.80+211509.2 (esdL1, red dashed line; data from Luhman & Sheppard 2014). The spectrum of J1249+3621 is normalized at 1.3 $\mu$m, and the comparison spectra are normalized to maximize agreement in the 1.0–1.3 $\mu$m range. The dwarf and subdwarf comparisons are offset for ease of comparison. Major spectral features are labeled, as are regions of strong telluric absorption at 1.35–1.5 and 1.75–1.85 $\mu$m (vertical gray bands). Right: comparison of the smoothed spectrum of J1249+3621 (black lines) to best-fit models (magenta lines) from the Sonora Elf Owl (top; Mukherjee et al. 2024) and SAND (bottom; Alvarado et al. 2024) atmosphere grids. Spectra are scaled to apparent fluxes using the UHS $J$-band magnitude of J1249+3621, and the models are scaled to minimize $\chi^2_r$. Model parameters are listed in the figure captions. Difference spectra (observed minus computed; black line) are compared to the $\pm1\sigma$ uncertainty of the observed flux densities (gray band) in the bottom panels.

the apparent spectral flux densities of J1249+3621, following the procedure described in Burgasser et al. (2024). Our best-fit models and parameters are shown in Figure 1. The Elf Owl and SAND grids yield distinctly different effective temperatures ($T_{\rm eff} = 2260 \pm 60$ K versus $1785 \pm 70$ K) and metallicities ([M/H] $= -0.63 \pm 0.10$ versus $-1.28 \pm 0.10$) but similar surface gravities (logg $= 4.66 \pm 0.11$ versus $4.88 \pm 0.24$). We note that the Elf Owl grid does not extend to [M/H] $< -1$ and does not include a prescription for condensate cloud formation, although the latter may be less important in metal-poor L subdwarf atmospheres (Burgasser et al. 2007; Gonzales et al. 2021). The best-fit Elf Owl model is a marginally better fit to the observed spectrum,[18] and its scaled surface fluxes are in good agreement with the spectrophotometric distance estimate ($d = 102$ pc) assuming a radius of $0.08\,R_\odot$. The model fit discrepancies could be resolved by a direct distance measurement. Nevertheless, this analysis confirms our interpretation of J1249+3621 as a low-temperature, metal-poor object. We note that the SAND models suggest significant alpha enrichment ([$\alpha$/Fe] $= +0.25 \pm 0.07$) and the Elf Owl models marginal C/O enrichment (C/O $= 0.71 \pm 0.16$), potential clues to the origin of this source.

Adopting generous parameter ranges of 1715 K $\lesssim T_{\rm eff} \lesssim$ 2320 K and $-1.4 \leqslant$ [M/H] $\leqslant -0.5$, and assuming an age $\tau \geqslant 5$ Gyr, the SAND evolutionary models (SANDee; Gerasimov et al. 2024) predict a mass of $0.082^{+0.002}_{-0.003}\,M_\odot$, placing this source marginally above the metallicity-dependent hydrogen-burning minimum mass (HBMM $\approx 0.080\,M_\odot$ for [M/H] $= -1$). The relatively narrow uncertainty range indicated by the evolutionary models is due to the steep decline in temperatures below the HBMM for old low-temperature sources and does not account for potential systematic biases (e.g., nonsolar abundance patterns). We conclude that J1249+3621 is likely a low-mass, metal-poor star, with a 10% probability of being a high-mass brown dwarf.

### 3.2. Radial Velocity and Kinematics

At full resolution, the Keck/NIRES data permit assessment of the radial velocity of J1249+3621, which we approached using a forward-modeling technique described in Burgasser et al. (2024). In brief, we fit the extracted NIRES spectrum without telluric correction to a high-resolution stellar atmosphere model, $M(\lambda)$, from Allard et al. (2012, BT-Settl) and an empirical telluric absorption template, $T(\lambda)$, from Livingston &

[18] The best fits yield $\chi^2_r = 9.4$ for Elf Owl and $\chi^2_r = 14.4$ for SAND, where $\chi^2_r = \chi^2/{\rm dof}$, with dof $= 263$. These values indicate a relative probability $\ln \mathcal{P} = -\chi^2_{r,{\rm SAND}}/\chi^2_{r,ElfOwl} = -1.5$ or $\mathcal{P} = 0.22$ that the models equally represent the data.

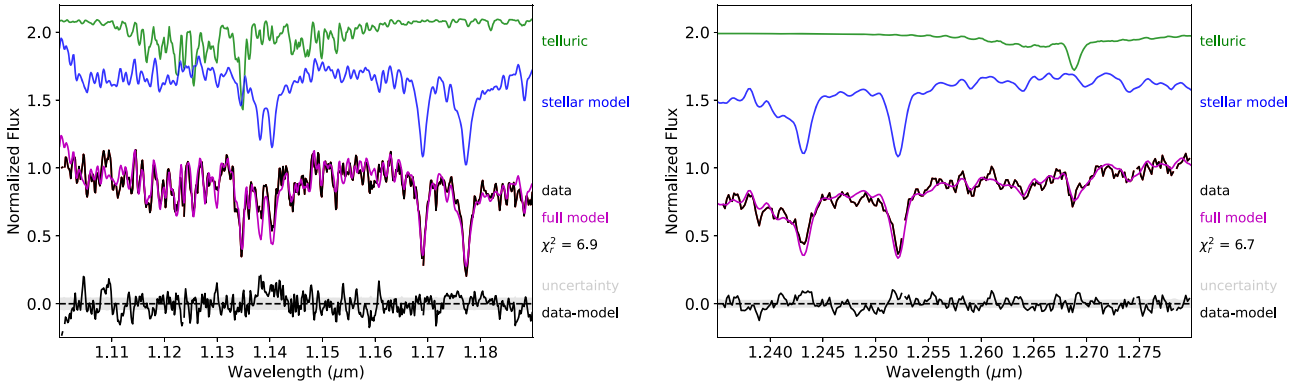


**Figure 2.** Forward modeling of the Keck/NIRES spectrum of J1249+3621 in the 1.10–1.19 $\mu$m (left) and 1.235–1.28 $\mu$m (right) spectral regions, both of which contain stellar and telluric absorption features. Each panel displays, from top to bottom, the telluric spectrum in green, the stellar model in blue, the combined model in magenta overlaid on the observed spectrum in black, and the difference spectrum (data model) in black overlaid on the $\pm$ 1$\sigma$ uncertainty band in gray. The reduced $\chi^2$ of each fit is indicated in the text to the right of the plot.

Wallace (1991) using the parameterized data model

$$D(\lambda + \delta_\lambda) = C(\lambda) \times [(M(\lambda^*) \otimes \kappa_R(v \sin i)) \times T^\alpha(\lambda)] \otimes \kappa_G(v_b) + \delta_f. \quad (1)$$

Here, $C(\lambda)$ is a fifth-order polynomial continuum correction, $\kappa_R(v \sin i)$ is a rotational broadening profile for projected velocity $v \sin i$, $\alpha$ is a scaling exponent for the strength of the telluric absorption, $\kappa_G(v_b)$ is a Gaussian instrumental broadening profile parameterized by velocity width $v_b$, and $\delta_\lambda$ and $\delta_f$ represent small offsets to the wavelength scale and normalized flux density to account for residual calibration errors. We used a $T_{\rm eff} = 2000$ K, $\log g = 5.0$, solar-metallicity model evaluated at a shifted wavelength $\lambda^* = \lambda\left(1 + \frac{RV + V_{\rm bary}}{c}\right)$, accounting for the unknown RV and known barycentric motion $v_{\rm bary} = 16.82$ km s$^{-1}$ at the time of observation. After identifying an optimized set of parameters using the Nelder–Mead algorithm (Nelder & Mead 1965) with a fixed $v \sin i = 50$ km s$^{-1}$, we used a Metropolis–Hastings MCMC algorithm to map the parameter uncertainty space for the five remaining free parameters: RV, $\alpha$, $v_b$, $\delta_\lambda$, and $\delta_f$. Fits were conducted in two wavelength regions that contain both stellar and telluric absorption features: 1.10–1.19 $\mu$m, which contains Na I (1.138, 1.140 $\mu$m) and K I (1.169, 1.177 $\mu$m) stellar lines and a telluric complex over 1.11–1.15 $\mu$m, and 1.235–1.28 $\mu$m, which contains K I stellar lines (1.243, 1.252 $\mu$m) and a telluric feature at 1.269 $\mu$m. We avoided the CO band at 2.3 $\mu$m, commonly used for RV forward modeling of L dwarfs (see Blake et al. 2010; Konopacky et al. 2010; Burgasser et al. 2015) due to the suppression of this feature by $H_2$ absorption. Figure 2 displays the best-fit models for these regions, which yield consistent values for RV ($-92^{+13}_{-14}$ km s$^{-1}$ and $-114^{+13}_{-14}$ km s$^{-1}$). We adopt a mean RV $= -103 \pm 10$ km s$^{-1}$ for J1249+3621.

Combining the measured RV, proper motion, and position of J1249+3621 with its estimated distance, we computed *UVW* velocities in the local standard of rest (LSR).[19] The velocities (Table 1) indicate a slightly retrograde motion relative to Galactic rotation ($V_{\rm LSR} = -292 \pm 19$ km s$^{-1}$), with a trajectory directed radially inward ($U_{\rm LSR} = 449 \pm 28$ km s$^{-1}$) and constrained to the Galactic disk ($W_{\rm LSR} = -15 \pm 11$ km s$^{-1}$). Assuming a local Galactic circular velocity of $v_{\rm circ} = 220$ km s$^{-1}$, the velocity of J1249+3621 translates into a Galactic rest frame (GRF) speed of $v_{\rm GRF} = 456 \pm 27$ km s$^{-1}$ or $0.47 \pm 0.03$ kpc Myr$^{-1}$. The median speed is just below the Galactic escape velocity at the Solar radius, with current estimates ranging from $521^{+46}_{-30}$ km s$^{-1}$ (Williams et al. 2017, 1.6$\sigma$ above) to $580 \pm 63$ km s$^{-1}$ (Monari et al. 2018; 1.8$\sigma$ above). Given the uncertainties in the inferred velocities and potential models, we find that J1249+3621 has a significant probability of being unbound to the Milky Way.

The Galactic orbit of J1249+3621 was generated using `galpy` (Bovy 2015). We used the axisymmetric MWPotential2014 potential to integrate the trajectory of J1249+3621 forward and backward in time by up to 10 Gyr, with a finer sampling of the backward orbit up to 150 Myr. We drew 100 random initial conditions sampling the uncertainties on distance, proper motion, and radial velocity assuming independent Gaussian distributions. Figure 3 displays the forward and backward trajectories projected onto the disk plane and in cylindrical coordinates. The forward motion of J1249+3621 shows a close approach to the inner region of the Milky Way, coming within $0.94^{+0.28}_{-0.19}$ kpc of the Galactic center, then extending beyond the Milky Way's virial radius of 180 kpc (Sylos Labini et al. 2023). The median model remains bound to the Milky Way on a $\sim$3 Gyr, highly eccentric orbit, but 17% of our simulated orbits are unbound over 10 Gyr. The backward orbit is approximately radial and tightly confined to the Galactic plane, converging to within 2° of $05^{\rm h}22^{\rm m}25^{\rm s}$ +38°37′ 00″ (Galactic coordinate $38\overset{\circ}{.}6$ $+1\overset{\circ}{.}2$) by 50 Myr in the past.

## 4. Assessing the Origins of J1249+3621

### 4.1. Was J1249+3621 Ejected from the Galactic Center?

J1249+3621 has a unique trajectory and speed; less than 0.002% of stars in Gaia within 200 pc of the Sun have comparable tangential velocities.[20] While this could nevertheless represent the extreme tail of the halo velocity distribution (Hawkins & Wyse 2018), we explored the potential origins of J1249+3621 in the context of currently known hypervelocity stars. Its small but nonzero orbital angular

[19] LSR velocity components assume a right-handed coordinate system centered on the Sun with *U* pointed radially inward, *V* pointed in the direction of Galactic rotation, and *W* pointed toward the north Galactic pole. We assumed solar velocity components of $(U_\odot, V_\odot, W_\odot) = (11.1$ km s$^{-1}$, 12.24 km s$^{-1}$, 7.25 km s$^{-1}$; Schönrich et al. 2010).

[20] This statistic is based on a search of Gaia DR3 for sources with $\pi > 5$ mas, $\pi/\sigma_\pi > 10$, and $v_{\rm tan} > 500$ km s$^{-1}$, which comprises 34 sources out of 2,234,316 without a tangential velocity constraint.

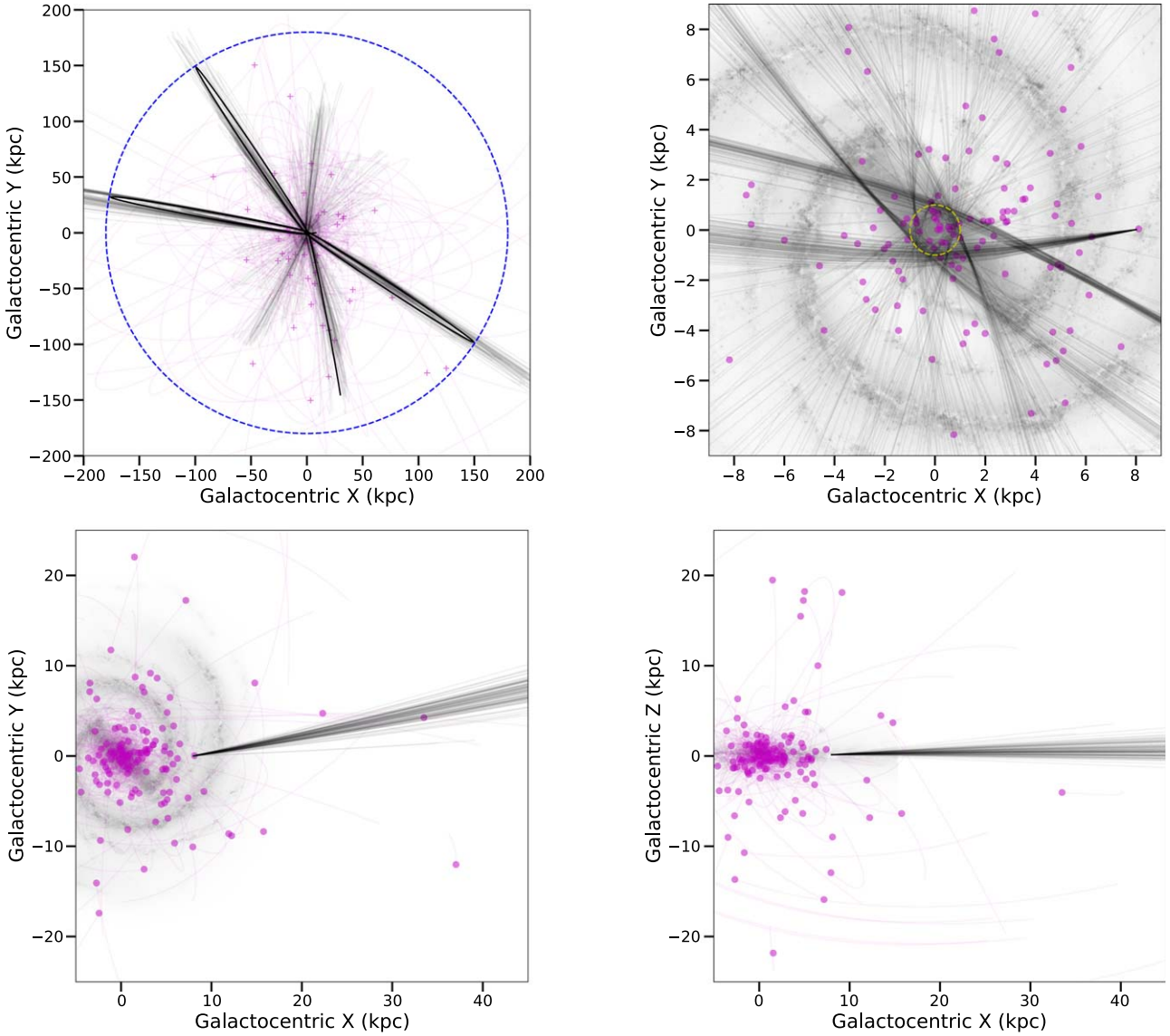


**Figure 3.** Projected orbit of J1249+3621 from `galpy` (Bovy 2015) for 100 initial conditions sampling uncertainties in distance, proper motion, and RV (black lines). The top panels display the forward orbit over 10 Gyr projected onto the Galactic plane on wide (left) and narrow (right) distance scales. The bottom panels display the backward orbit over 150 Myr projected onto the Galactic plane (left) and *XZ* coordinates (right). The top-left panel shows the present-day positions (magenta crosses) and forward-projected orbits (magenta lines) of 50 satellite galaxies from Fritz et al. (2018), as well as the Milky Way's virial radius of 180 kpc (dashed blue circle; Sylos Labini et al. 2023). The top-right panel shows the present-day positions of 161 GCs from Vasiliev (2019; magenta circles) and the closest-approach radius of ∼1 kpc from the Galactic center (yellow dashed circle). GCs and their backward-projected orbits (magenta lines) are also shown in the bottom panels.

momentum in the GRF ($L_z = 572^{+147}_{-146}$ kpc km s$^{-1}$) and inward trajectory would seem to argue against ejection from the Galactic center through the traditional Hill's mechanism (Hills 1988). However, if J1249+3621 is bound to the Milky Way, which is the case for 83% of our orbit simulations, we could be observing it on a return pass after intervals of roughly 3 Gyr, with torques imparted by asymmetries in the Galactic potential, i.e., the spiral structure or the inner bar (Sellwood & Binney 2002; Daniel & Wyse 2018). Moreover, while the majority of Galactic center stars are metal rich (Carr et al. 2000; Ramírez et al. 2000; Cunha et al. 2007), recent studies have identified metal-poor, alpha-enhanced M giants in the nuclear region similar in nature to J1249+3621 (Schultheis et al. 2015, 2020). A small number of metal-poor hypervelocity stars have also been associated with ejection from the Galactic center (Li et al. 2012, 2023). Thus, despite its radially inward trajectory, ejection via the Hill's mechanism is a possible origin for J1249+3621.

### *4.2. Is J1249+3621 the Surviving Companion of a Type Ia Supernova?*

An alternative disk origin for J1249+3621 is as the tight binary companion to an accreting white dwarf that exceeded the 1.4 $M_\odot$ Chandrasekhar limit (Chandrasekhar 1931, 1935), underwent a thermonuclear explosion, and released J1249+3621 at high speed (Blaauw 1961; Portegies Zwart 2000; Shen et al. 2018). Several accreting short-period white dwarf–brown dwarf pairs (polars and cataclysmic variables) are known with white dwarf masses extending up to 0.94 $M_\odot$ (Longstaff et al. 2019 and references therein). If J1249+3621 was the initially more massive donor in such a system, its

subsequent ejection speed would exceed $690\left(\frac{P}{1\ hr}\right)^{-1/3}$ km s$^{-1}$ based on orbital motion alone, where $P$ is the orbit period at detonation. Periods of 1–1.5 hr are sufficient for Roche lobe overflow[21] for donors near the HBMM, based on theory and as observed for low-mass cataclysmic variables (e.g., Kolb & Baraffe 1999; Littlefair et al. 2006). This scaling law yields ejection speeds of 550–700 km s$^{-1}$, on par with J1249+3621's LSR speed of 534 km s$^{-1}$. Contributions from supernova shockwaves and mass stripping could drive ejection velocities even higher (Pan et al. 2012; Rau & Pan 2022).

As the ejection direction in this scenario is isotropic, the probability of an individual source such as J1249+3621 passing by the Sun is very low. However, the overall higher density of stars in the Galactic plane makes it more likely that we would see a closely passing ejectee with a trajectory confined to the plane. We note that there are no known supernova remnants in the projected past position of J1249 +3621, but as remnants dissipate and merge with the interstellar medium within $\lesssim$1 Myr (Leahy & Williams 2017), this a relatively weak constraint on the time since this source could have been ejected.

### 4.3. Was J1249+3621 Ejected from a Globular Cluster?

Another possible origin for J1249+3621 is dynamical ejection from a globular cluster. The top-heavy present-day mass functions of these clusters are evidence of efficient tidal dispersion of low-mass objects (Fregeau et al. 2002), and large velocity kicks exceeding the 10–100 km s$^{-1}$ escape velocities of GCs are a natural outcome of strong three- and four-body dynamical interactions that are commonplace in these systems (Leonard 1991). Such kicks are amplified by interactions with black hole binaries (Cabrera & Rodriguez 2023), which are now understood to dominate the dynamics of the centers of most GCs (Kremer et al. 2020a). The characteristic kick velocity imparted to a star of mass $m$ during a strong encounter with a binary with components of equal mass $M$ and semimajor axis $a$ is roughly

$$v_{\rm kick} \approx \sqrt{\frac{GM^2}{ma}} \approx 600\left(\frac{M}{20\ M_\odot}\right)\left(\frac{m}{0.1\ M_\odot}\right)^{-1/2} \times \left(\frac{a}{10\ {\rm au}}\right)^{-1/2} {\rm km\ s^{-1}}. \quad (2)$$

Thus, for $a \lesssim 10$ au and/or compact object masses $M \gtrsim 20\ M_\odot$, sufficiently high velocities can be achieved.

To test this mechanism, we searched for low-mass, high-velocity stars in the `CMC Cluster Catalog` (Kremer et al. 2020b), a public suite of $N$-body simulations intended to serve as a proxy for the Galactic GC population (Harris 1996). These simulations adopt a Kroupa (2001) initial mass function ranging from 0.08 to 150 $M_\odot$ and therefore include stars of mass comparable to J1249+3621. At times $t > 8$ Gyr, typical of the ages of Milky Way GCs, we identify roughly 4000 low-mass stars ($M < 0.2\ M_\odot$) ejected with velocities of at least 100 km s$^{-1}$, corresponding to a rate of roughly 1 Myr$^{-1}$ across the Milky Way. Of these, 6 stars are ejected with $V > 500$ km s$^{-1}$, corresponding to a rate of roughly 2 Gyr$^{-1}$. All six hypervelocity subdwarfs are ejected via dynamical encounters with stellar-mass black hole binaries with properties similar to the scales in Equation (2). Hence, simulations support the scenario of GC ejection as a means of generating very high-velocity, very low-mass objects, albeit as exceedingly rare events. The isotropic distribution of ejections further reduces the probability of this scenario, with the same caveat that the higher concentration of GCs in the Galactic plane makes detection of closely passing ejectees on planar orbits more likely.

There are no known GCs within 5° of the projected past position of J1249+3621. However, given the long timescales involved it is necessary to account for cluster motion. We used our `galpy` orbits to assess whether the trajectory of J1249 +3621 intersected with any of the 161 GCs in the kinematic catalog of Vasiliev (2019), projecting all orbits back 150 Myr. The closest approaches by NGC 3201 and Palomar 1 are more than 4 kpc in separation, making these improbable origin sites. The low Galactic latitude of the projected past position of J1249+3621 ($b = +1\overset{\circ}{.}2$) could argue for an origin from an as-yet-undiscovered GC hidden in the Galactic plane. Alternately, the higher concentration of GCs near the Galactic center implies that J1249+3621 could have been ejected from one of these systems and is now making a return pass $\gtrsim$3 Gyr later. Despite these considerations, we find the GC ejection scenario less likely than the prior two scenarios.

For completeness, we note that four open clusters lie within 1° of the projected past position of J1249+3621, including the well-studied NGC 1857 system at 3.1 kpc (Herschel 1864). However, the lower stellar densities of these systems and lack of compact binaries from massive progenitors make dynamic ejection unlikely, and none of these clusters have significantly subsolar metallicities characteristic of J1249+3621.

### 4.4. Is J1249+3621 an Extragalactic Star?

As the bound orbits of J1249+3621 extend beyond the Milky Way's virial radius, it is possible that this source could have an extragalactic origin, specifically accretion from one of the Milky Way satellites (Abadi et al. 2009; Piffl et al. 2011). Its present trajectory does not align with distant extragalactic systems such as M31 or the Magellanic Clouds. We examined the intersection of J1249+3621's orbit with 50 Milky Way satellites from Fritz et al. (2018) using the same procedure as our GCs, integrating back to 10 Gyr. Only one system, Tucana III (Drlica-Wagner et al. 2015), comes within 5 kpc of the median orbit of J1249+3621 about 6 Gyr ago. The substantial uncertainties of the trajectories of J1249+3621 and the known dwarf satellites over Gyr timescales mean we cannot strictly rule out this scenario; however, we find it the least likely of the scenarios considered here, given that the trajectory of J1249 +3621 is confined to the Galactic plane.

Inferring the true origin of J1249+3621 will require further investigation into its physical and atmospheric properties. A Galactic center origin requires closer examination of its orbital trajectory through refinement of its distance (by direct parallax measurement) and velocity components, as well as a more realistic, nonaxisymmetric Galactic potential model. A more detailed compositional analysis would also help clarify its origin. For example, if J1249+3621 is the surviving companion of a Type Ia supernova, its atmosphere may be enriched with heavy elements, particularly nickel, depending on the degree of mass stripping by the supernova blast wave (Rau &

[21] Following Eggleton (1983), $a/R_* \approx$ 3–10 for a star-white dwarf system that evolves from 0.6 $M_\odot$+0.9 $M_\odot$ to 0.1 $M_\odot$+1.4 $M_\odot$, where $a$ is the orbit semimajor axis and $R_*$ the radius of the mass donor. In the latter configuration, $P \approx$ 1–1.5 hr for average densities of 50–80 g cm$^{-3}$.

Pan 2022). Similarly, if J1249+3621 was ejected from the Galactic center, a GC, or a satellite system, its detailed abundances may provide the chemical fingerprint of its origin. Better assessment of composition through additional optical and infrared spectra and improved atmosphere models exploring specific abundances (e.g., Gerasimov et al. 2022) are needed to infer a chemical-based origin.

Finally, we note that at least one other metal-poor L subdwarf, the esdL1 ULAS J231949.36+044559.5 (Zhang et al. 2018), has a high-enough estimated tangential velocity ($513^{+50}_{-46}$ km s$^{-1}$) to make it a promising hypervelocity candidate, although no RV has yet been reported for this source. The existence of at least one and possibly two L subdwarfs within ~200 pc of the Sun with hypervelocity speeds suggests a considerably larger population of such sources could exist in the Milky Way system.

## Acknowledgments

We thank Keck Observatory staff Randy Campbell and Max Service for their support during the Keck/NIRES observations. Figure 3 was made with the MWplot package created by Henry Leung (https://github.com/henrysky/milkyway_plot) and graphics created by Robert Hurt (https://www.spitzer.caltech.edu/image/ssc2008-10a-a-roadmap-to-the-milky-way). The authors acknowledge the helpful discussions with Boris Gaensickle and Keith Hawkins in the preparation of this manuscript and a prompt and helpful review by our anonymous referee. This material is based upon work supported by the National Science Foundation under grant No. 2009136. Support for K. K. was provided by NASA through the NASA Hubble Fellowship grant HST-HF2-51510 awarded by the Space Telescope Science Institute, which is operated by the Association of Universities for Research in Astronomy, Inc., for NASA under contract NAS5-26555. This publication makes use of data products from the Wide-field Infrared Survey Explorer, which is a joint project of the University of California, Los Angeles, and the Jet Propulsion Laboratory/California Institute of Technology, and NEOWISE, which is a project of the Jet Propulsion Laboratory/California Institute of Technology. WISE and NEOWISE are funded by the National Aeronautics and Space Administration. This research has benefited from the SpeX Prism Libraries Analysis Toolkit, maintained by Adam Burgasser at https://github.com/aburgasser/splat. This research has made use of the SIMBAD database (Wenger et al. 2000), the "Aladin sky atlas" (Bonnarel et al. 2000), and the VizieR catalog access tool developed and operated at CDS, Strasbourg, France. The data presented herein were obtained at Keck Observatory, which is a private 501(c)3 nonprofit organization operated as a scientific partnership among the California Institute of Technology, the University of California, and the National Aeronautics and Space Administration. The Observatory was made possible by the generous financial support of the W. M. Keck Foundation. The authors recognize and acknowledge the significant cultural role and reverence that the summit of Maunakea has within the indigenous Hawaiian community and that the W. M. Keck Observatory stands on Crown and Government Lands that the State of Hawaii is obligated to protect and preserve for future generations of indigenous Hawaiians. Portions of this work were conducted at the University of California, San Diego, which was built on the unceded territory of the Kumeyaay Nation, whose people continue to maintain their political sovereignty and cultural traditions as vital members of the San Diego community.

*Facility:* Keck:II (NIRES).

*Software:* astropy (Astropy Collaboration et al. 2013, 2018, 2022), Matplotlib (Hunter 2007), NumPy (van der Walt et al. 2011), pandas (Wes McKinney 2010), SciPy (Virtanen et al. 2020), SpeXTool (Cushing et al. 2004), SPLAT (Burgasser & Splat Development Team 2017).

## ORCID iDs

Adam J. Burgasser https://orcid.org/0000-0002-6523-9536
Roman Gerasimov https://orcid.org/0000-0003-0398-639X
Kyle Kremer https://orcid.org/0000-0002-4086-3180
Hunter Brooks https://orcid.org/0000-0002-5253-0383
Efrain Alvarado, III https://orcid.org/0009-0005-8159-8490
Adam C. Schneider https://orcid.org/0000-0002-6294-5937
Aaron M. Meisner https://orcid.org/0000-0002-1125-7384
Christopher A. Theissen https://orcid.org/0000-0002-9807-5435
Emma Softich https://orcid.org/0000-0002-1420-1837
Preethi Karpoor https://orcid.org/0000-0002-1480-9041
Thomas P. Bickle https://orcid.org/0000-0003-2235-761X
Martin Kabatnik https://orcid.org/0000-0003-4905-1370
Austin Rothermich https://orcid.org/0000-0003-4083-9962
Dan Caselden https://orcid.org/0000-0001-7896-5791
J. Davy Kirkpatrick https://orcid.org/0000-0003-4269-260X
Jacqueline K. Faherty https://orcid.org/0000-0001-6251-0573
Sarah L. Casewell https://orcid.org/0000-0003-2478-0120
Marc J. Kuchner https://orcid.org/0000-0002-2387-5489

## References

Abadi, M. G., Navarro, J. F., & Steinmetz, M. 2009, ApJL, 691, L63
Allard, F., Homeier, D., & Freytag, B. 2012, RSPTA, 370, 2765
Alvarado, E., Gerasimov, R., Burgasser, A. J., et al. 2024, RNAAS, 8, 134
Astropy Collaboration, Robitaille, T. P., Tollerud, E. J., et al. 2013, A&A, 558, A33
Astropy Collaboration, Price-Whelan, A. M., Sipőcz, B. M., et al. 2018, AJ, 156, 123
Astropy Collaboration, Price-Whelan, A. M., Lim, P. L., et al. 2022, ApJ, 935, 167
Bardalez Gagliuffi, D. C., Burgasser, A. J., Gelino, C. R., et al. 2014, ApJ, 794, 143
Blaauw, A. 1961, BAN, 15, 265
Blake, C. H., Charbonneau, D., & White, R. J. 2010, ApJ, 723, 684
Bonnarel, F., Fernique, P., Bienaymé, O., et al. 2000, A&AS, 143, 33
Bovy, J. 2015, ApJS, 216, 29
Brooks, H., Kirkpatrick, J. D., Caselden, D., et al. 2022, AJ, 163, 47
Brown, W. R. 2015, ARA&A, 53, 15
Burgasser, A. J., Cruz, K. L., & Kirkpatrick, J. D. 2007, ApJ, 657, 494
Burgasser, A. J. & Splat Development Team 2017, Astronomical Society of India Conf. Ser. Proc. of the Int. Workshop on Stellar Spectral Libraries (IWSSL 2017)14ed. P. Coelho, L. Martins, & E. Griffin, (Bangalore: Astronomical Society of India), 7
Burgasser, A. J., Kirkpatrick, J. D., Burrows, A., et al. 2003, ApJ, 592, 1186
Burgasser, A. J., Gillon, M., Melis, C., et al. 2015, AJ, 149, 104
Burgasser, A. J., Schneider, A. C., Meisner, A. M., et al. 2024, ApJ, submitted
Cabrera, T., & Rodriguez, C. L. 2023, ApJ, 953, 19
Carr, J. S., Sellgren, K., & Balachandran, S. C. 2000, ApJ, 530, 307
Chambers, K. C., Magnier, E. A., Metcalfe, N., et al. 2016, arXiv:1612.05560
Chandrasekhar, S. 1931, MNRAS, 91, 456
Chandrasekhar, S. 1935, MNRAS, 95, 207
Cui, X.-Q., Zhao, Y.-H., Chu, Y.-Q., et al. 2012, RAA, 12, 1197
Cunha, K., Sellgren, K., Smith, V. V., et al. 2007, ApJ, 669, 1011
Cushing, M. C., Vacca, W. D., & Rayner, J. T. 2004, PASP, 116, 362
Daniel, K. J., & Wyse, R. F. G. 2018, MNRAS, 476, 1561

Drlica-Wagner, A., Bechtol, K., Rykoff, E. S., et al. 2015, ApJ, 813, 109
Du, C., Li, H., Yan, Y., et al. 2019, ApJS, 244, 4
Dye, S., Lawrence, A., Read, M. A., et al. 2018, MNRAS, 473, 5113
Eggleton, P. P. 1983, ApJ, 268, 368
Favia, A., West, A. A., & Theissen, C. A. 2015, ApJ, 813, 26
Fragione, G., & Gualandris, A. 2019, MNRAS, 489, 4543
Fregeau, J. M., Joshi, K. J., Portegies Zwart, S. F., & Rasio, F. A. 2002, ApJ, 570, 171
Fritz, T. K., Battaglia, G., Pawlowski, M. S., et al. 2018, A&A, 619, A103
Gaia Collaboration, Brown, A. G. A., Vallenari, A., et al. 2021, A&A, 650, C3
Gerasimov, R., Bedin, L. R., Burgasser, A. J., et al. 2024, arXiv:2405.01634
Gerasimov, R., Burgasser, A. J., Homeier, D., et al. 2022, ApJ, 930, 24
Gonzales, E. C., Burningham, B., Faherty, J. K., et al. 2021, ApJ, 923, 19
Gonzales, E. C., Faherty, J. K., Gagné, J., Artigau, É., & Bardalez Gagliuffi, D. 2018, ApJ, 864, 100
Harris, W. E. 1996, AJ, 112, 1487
Hastings, W. K. 1970, Biometrika, 57, 97
Hawkins, K., & Wyse, R. F. G. 2018, MNRAS, 481, 1028
Herschel, J. F. W. 1864, RSPT, 154, 1
Hills, J. G. 1988, Natur, 331, 687
Hunter, J. D. 2007, CSE, 9, 90
Kirkpatrick, J. D., Looper, D. L., Burgasser, A. J., et al. 2010, ApJS, 190, 100
Kirkpatrick, J. D., Marocco, F., Caselden, D., et al. 2021a, ApJL, 915, L6
Kirkpatrick, J. D., Gelino, C. R., Faherty, J. K., et al. 2021b, ApJS, 253, 7
Kolb, U., & Baraffe, I. 1999, MNRAS, 309, 1034
Konopacky, Q. M., Ghez, A. M., Barman, T. S., et al. 2010, ApJ, 711, 1087
Kremer, K., Ye, C. S., Chatterjee, S., Rodriguez, C. L., & Rasio, F. A. 2020a, in IAU Symp. 351, Star Clusters: From the Milky Way to the Early Universe, ed. A. Bragaglia (Cambridge: Cambridge Univ Press), 357
Kremer, K., Ye, C. S., Rui, N. Z., et al. 2020b, ApJS, 247, 48
Kroupa, P. 2001, MNRAS, 322, 231
Kuchner, M. J., Faherty, J. K., Schneider, A. C., et al. 2017, ApJL, 841, L19
Lang, D. 2014, AJ, 147, 108
Leahy, D. A., & Williams, J. E. 2017, AJ, 153, 239
Leonard, P. J. T. 1991, AJ, 101, 562
Li, Q.-Z., Huang, Y., Dong, X.-B., et al. 2023, AJ, 166, 12
Li, Y., Luo, A., Zhao, G., et al. 2012, ApJL, 744, L24
Liao, J., Du, C., Li, H., Ma, J., & Shi, J. 2023, ApJL, 944, L39
Linsky, J. L. 1969, ApJ, 156, 989
Littlefair, S. P., Dhillon, V. S., Marsh, T. R., et al. 2006, Sci, 314, 1578
Livingston, W., & Wallace, L. 1991, An Atlas of the Solar Spectrum in the Infrared from 1850 to 9000 $cm^{-1}$ (1.1 to 5.4 Micrometer) (Tucson, AZ: National Solar Observatory)
Longstaff, E. S., Casewell, S. L., Wynn, G. A., et al. 2019, MNRAS, 484, 2566
Luhman, K. L., & Sheppard, S. S. 2014, ApJ, 787, 126
Mainzer, A., Bauer, J., Cutri, R. M., et al. 2014, ApJ, 792, 30
Majewski, S. R., Schiavon, R. P., Frinchaboy, P. M., et al. 2017, AJ, 154, 94
Marocco, F., Eisenhardt, P. R. M., Fowler, J. W., et al. 2021, ApJS, 253, 8
Meisner, A. M., Lang, D., & Schlegel, D. J. 2018, AJ, 156, 69
Meisner, A. M., Faherty, J. K., Kirkpatrick, J. D., et al. 2020, ApJ, 899, 123
Meisner, A. M., Schneider, A. C., Burgasser, A. J., et al. 2021, ApJ, 915, 120
Metropolis, N., Rosenbluth, A. W., Rosenbluth, M. N., Teller, A. H., & Teller, E. 1953, JChPh, 21, 1087
Monari, G., Famaey, B., Carrillo, I., et al. 2018, A&A, 616, L9
Mukherjee, S., Fortney, J. J., Morley, C. V., et al. 2024, ApJ, 963, 73
Nelder, J. A., & Mead, R. 1965, CompJ, 7, 308
Pan, K.-C., Ricker, P. M., & Taam, R. E. 2012, ApJ, 750, 151
Piffl, T., Williams, M., & Steinmetz, M. 2011, A&A, 535, A70
Portegies Zwart, S. F. 2000, ApJ, 544, 437
Quispe-Huaynasi, F., Roig, F., McDonald, D. J., et al. 2022, AJ, 164, 187
Ramírez, S. V., Sellgren, K., Carr, J. S., et al. 2000, ApJ, 537, 205
Rau, S.-J., & Pan, K.-C. 2022, ApJ, 933, 38
Schlafly, E. F., Meisner, A. M., & Green, G. M. 2019, ApJS, 240, 30
Schneider, A. C., Burgasser, A. J., Gerasimov, R., et al. 2020, ApJ, 898, 77
Scholz, R.-D. 2024, A&A, 685, A162
Schönrich, R., Binney, J., & Dehnen, W. 2010, MNRAS, 403, 1829
Schultheis, M., Cunha, K., Zasowski, G., et al. 2015, A&A, 584, A45
Schultheis, M., Rojas-Arriagada, A., Cunha, K., et al. 2020, A&A, 642, A81
Sellwood, J. A., & Binney, J. J. 2002, MNRAS, 336, 785
Shen, K. J., Boubert, D., Gänsicke, B. T., et al. 2018, ApJ, 865, 15
Steinmetz, M., Zwitter, T., Siebert, A., et al. 2006, AJ, 132, 1645
Sylos Labini, F., Chrobáková, Ž., Capuzzo-Dolcetta, R., & López-Corredoira, M. 2023, ApJ, 945, 3
Vacca, W. D., Cushing, M. C., & Rayner, J. T. 2003, PASP, 115, 389
van der Walt, S., Colbert, S. C., & Varoquaux, G. 2011, CSE, 13, 22
Vasiliev, E. 2019, MNRAS, 484, 2832
Virtanen, P., Gommers, R., Oliphant, T. E., et al. 2020, NatMe, 17, 261
Wenger, M., Ochsenbein, F., Egret, D., et al. 2000, A&AS, 143, 9
Wes McKinney 2010, in Proc. of the Python in Science Conf., Data Structures for Statistical Computing in Python9ed. S. van der Walt & J. Millman, 61
Williams, A. A., Belokurov, V., Casey, A. R., & Evans, N. W. 2017, MNRAS, 468, 2359
Wilson, J. C., Henderson, C. P., Herter, T. L., et al. 2004, Proc. SPIE, 5492, 1295
Wright, E. L., Eisenhardt, P. R. M., Mainzer, A. K., et al. 2010, AJ, 140, 1868
Yu, Q., & Tremaine, S. 2003, ApJ, 599, 1129
Zhang, Z. H., Burgasser, A. J., Gálvez-Ortiz, M. C., et al. 2019, MNRAS, 486, 1260
Zhang, Z. H., Pinfield, D. J., Gálvez-Ortiz, M. C., et al. 2017, MNRAS, 464, 3040
Zhang, Z. H., Galvez-Ortiz, M. C., Pinfield, D. J., et al. 2018, MNRAS, 480, 5447